Seasonal Prediction of the Leeuwin Current using the POAMA Dynamical Seasonal Forecast Model

Harry H. Hendon[1] and Guomin Wang

Centre for Australian Weather and Climate Research*

Melbourne, Australia

30 June 2008

*A partnership between the Bureau of Meteorology and the Commonwealth Scientific and Industrial Research Organization

[1] Corresponding author: H.H. Hendon, CAWCR, Bureau of Meteorology, PO Box 1289, Melbourne, 3001 Australia. Email hhh@bom.gov.au

Abstract

The potential for prediction of interannual variations of the Leeuwin Current along the west coast of Australia is addressed. The Leeuwin Current flows poleward against the prevailing winds and transports warm-fresh tropical water southward along the coast, which has a great impact on local climate and ecosystems. Variations of the current are tightly tied to El Niño/La Niña (weak during El Niño and strong during La Niña). Skilful seasonal prediction of the Leeuwin Current to nine month lead time was achieved by empirical downscaling of forecasts of upper ocean heat content on the north west shelf of Australia from the POAMA seasonal forecast system. Prediction of the Leeuwin Current is possible because the heat content fluctuations on the north west shelf are the primary driver of interannual annual variations of the current and these heat content variations are tightly tied to the occurrence of El Niño/La Niña. POAMA can skilfully predict both the occurrence of El Niño/La Niña and the subsequent transmission of the heat content anomalies in the Pacific onto the north west shelf of Australia via the Indonesian throughflow.

1. Introduction

Dynamical seasonal prediction using coupled atmosphere-ocean general circulation models (AOGCM) is routinely performed at national and international forecast and research centres (e.g., Goddard et al. 2001). The foundation for predictions with such systems is the proven ability to predict the state of El Niño/Southern Oscillation (ENSO) at lead times up to about 12 months (Latif et al. 1998; Brankovic et al. 1994; Stockdale et al. 1998). Regional predictive skill outside of the tropical Pacific is primarily associated with atmospheric teleconnections to ENSO, which the coupled climate models presumably faithfully simulate. Most of the focus for application of dynamical seasonal prediction has been on exploiting the ability to predict the atmospheric teleconnections associated with ENSO, for obvious reasons. This note addresses the potential for dynamical seasonal prediction of an oceanic teleconnection of ENSO, namely interannual variations of the poleward flowing Leeuwin Current along the west coast of Australia (e.g., Pearce and Phillips 1988). We will demonstrate that interannual variations of the Leeuwin Current, which are of enormous economic and ecologic importance, are perhaps the most predictable component of the atmosphere-ocean climate system outside of the tropical Pacific due to the tight coupling to ENSO. We will demonstrate that skilful seasonal predictions of the Leeuwin Current, based on statistical downscaling of dynamical coupled model predictions of ENSO and its oceanic teleconnection into the Indian Ocean, are indeed possible.

2. Leeuwin Current

We begin by providing some background on the dynamics and importance of the Leeuwin Current. Unlike the prominent equatorward flowing eastern boundary currents along the western coasts of the Americas and Africa, the Leeuwin Current flows poleward against the prevailing winds, transporting warm and fresh water south along the subtropical west

coast of Australia (e.g., Smith et al. 1991b). The current is confined above about 300 m and is strongest at the surface. The Leeuwin Current displays pronounced mesoscale meanders and eddies (e.g., Legeckis and Cresswell 1981) but in the annual mean it appears as a narrow, coastally trapped, current flowing southward along the west Australian Coast from the Northwest Cape to Cape Leeuwin (Fig. 1a). Mean upper-ocean currents (averaged surface to 300 m depth) used in Fig. 1 are obtained from the POAMA Ocean Data Assimilation (Wang et al. 2002) and the sea surface temperatures (SST) are obtained from the analyses of Reynolds et al. (2002). We use data for the period 1982-2006. The current exhibits a pronounced annual variation in strength, with peak volume transport ~ 5 Sv and peak velocity ~0.5 ms^{-1} occurring in winter when the equatorward component of the mean wind is weakest (Smith et al. 1991b).

As a consequence of the Leeuwin Current, mean SST along the west coast of Australia (Fig. 1a) and mean rainfall in south west Western Australia are substantially higher than at similar subtropical latitudes along the west coasts of the Americas and Africa (e.g., Feng et al. 2003). The transport of relatively fresh tropical water south along the coast also results in the appearance of many aquatic species (plant and fish) at higher latitudes than would otherwise be the case. Interannual variations of the current have profound and predictable impacts on a number of important fisheries (e.g., Pearce and Phillips 1988).

The Leeuwin Current is thought to exist because the easterly trade winds in the Pacific force warm, low density tropical Pacific water into the eastern tropical Indian Ocean via the Indonesian Throughflow. As a result, a large-scale south-north pressure (i.e., steric height) gradient in the south eastern Indian Ocean is maintained. This large-scale south-north pressure gradient generates broad eastward (onshore) geostrophic transport that overcomes the locally-driven offshore Ekman transport and downwells on the coast. The southward flowing Leeuwin Current is in geostrophic balance with the resulting near-shore west-east

pressure gradient (e.g., Godfrey and Ridgway 1985). Variations of the current on annual to interannual time scales are coastally trapped (e.g., Feng et al. 2003). Variations in current strength can be monitored by sea level variations on the inshore side of the current. Feng et al. (2003) show that the sea level variation at Fremantle (32.06 °S, 115.75 °E) is linearly related to the volume transport of the current at the latitude of Fremantle and can be used to monitor the transport over a much winder geographical domain. Hence, we use Fremantle sea level variation, which has been measured continuously for over 100 years, as a proxy for variations of the overall strength of Leeuwin Current.

Interannual variation of the volume transport by the Leeuwin Current is dominated by ENSO (weak in El Niño years and strong in La Niña years; e.g., Pearce and Phillips 1988; Feng et al. 2003). This relationship is demonstrated in Fig. 2a, which shows the monthly time series of the Niño3.4 SST anomaly together with the observed sea level anomaly (smoothed with a running 3-month mean) at Fremantle (hereafter FSLA) for the period 1982-2005. Anomalies were formed by removal of the mean monthly seasonal cycle. The correlation between anomalies of Nino3.4 and FSLA is ~0.75 at zero lag.

This tight coupling of variations of the Leeuwin Current with ENSO stems from the transmission of the upper ocean heat content anomaly in the western Pacific (high during La Niña and low during El Niño) through the throughflow and southward along the Australian coast as a coastally trapped wave (e.g., Clarke and Liu 1994). This mechanism of variability is demonstrated in Fig. 3a, which shows the correlation of monthly FSLA with anomalies of upper ocean heat content.. High correlation extends locally up the west coast of Australia with a pattern similar to that shown by Feng et al. (2003) who used satellite altimeter sea surface height rather than upper ocean heat content. The high correlation appears to be coastally trapped south of the North West Cape (22°S, 115°E) and extends northward onto the northwest shelf of Australia and into the Indonesian seas and the tropical western Pacific.

A region of oppositely signed correlation occurs in the tropical eastern Pacific. This pattern of correlation in upper ocean heat content in the tropical Pacific is indicative of mature La Niña conditions. Hence, high sea level at Fremantle, or, equivalently, a strong Leeuwin Current is associated with La Niña conditions.

The transmission of the heat content anomaly from the Pacific onto the west coast of Australia during ENSO (e.g. Clarke and Liu 1994) is demonstrated in Fig. 4, which shows the lag correlation of seasonal mean upper ocean heat content anomalies with respect to the December-January-February mean Nino3.4 SST anomaly. As El Niño develops in the Pacific, off equatorial, westward propagating, upwelling Rossby waves impinge on the western boundary (Fig. 4a). Anomalously low heat content (elevated thermocline) then travels southward through the Indonesian throughflow (Figs. 4b) and onto the west Australian coast (Fig. 4c), eventually making it all the way around Cape Leeuwin and onto the south Australian coast (Fig. 4d). ENSO evolution is also associated with development of significant heat content anomalies in the equatorial Indian Ocean, which is a reflection of dynamical adjustment of the Indian Ocean to local wind forcing and is characteristic of the evolution of the Indian Ocean dipole that often accompanies development of ENSO (e.g., Shinoda et al. 2004a). These equatorial Indian Ocean heat content anomalies, which are a response to the near-equatorial zonal wind variations in the Indian Ocean that are primarily forced by the SST anomalies associated with ENSO in the Pacific (e.g., Shinoda et al. 2004b), do not play a role in variations of the Leeuwin Current or in variations of heat content on the west Australian Coast (e.g., Wiffels and Meyers 2003).

The impact of interannual variations of the Leeuwin Current on local SST along the west coast of Australia is demonstrated by the correlation of FSLA with SST (Fig. 1b). Also shown in Fig. 1b is the regression of mean upper ocean currents onto FSLA. A positive Leeuwin Current anomaly (positive FSLA) is associated with a coherent region of strong

positive SST correlation (peak correlation exceeding 0.6) along the entire subtropical west coast of Australia and extending north-westward into the south east tropical Indian Ocean. This pattern of SST correlation nicely delineates the geographic domain and regional impact of the Leeuwin Current: An anomalously strong current, which originates ~30º longitude off shore of the North West Cape and intensifies and contracts onto the coast to the south, appears to be associated with anomalous poleward advection of the mean south-to-north SST gradient. The variation of the upper ocean currents associated with interannual variations of FSLA (Fig. 1b) appears to be less coastally trapped than the mean Leeuwin Current (Fig. 1a), however, the breadth of the interannual current variation matches well the breadth of the associated SST anomaly (Fig. 1b). Feng et al. (2003), using in situ observations, indicate that interannual variations of the Leeuwin Current are as coastally trapped as is the mean current. Although there is a qualitative agreement between the breadth of the SST anomaly and breath of the anomalous current (Fig. 1b), the reduced coastal trapping for the interannual variations of the currents may reflect inadequacies in the depiction of the currents by the POAMA ocean assimilation/analyses. Computation of similar correlations using other available ocean analyses may provide additional insight.

3. Dynamic Seasonal Prediction with POAMA

Ideally, coupled climate models would have sufficient resolution and physics to allow direct prediction of the current variations along the western Australian coast but the modest resolution of the models used for seasonal prediction is far below that required to resolve the detailed dynamics that govern the Leeuwin Current (e.g., Reason et al. 1999). Hence, we focus on prediction of large-scale heat content variations on the northwest shelf of Australia that are at the heart of the variations of the current further to the south (Figs. 3a). The utility of using heat content averaged on the northwest shelf (15ºS-25ºS, 112ºE-120ºE; hereafter NWHC) as a proxy for Leeuwin Current variations is demonstrated in Fig. 2a. The

simultaneous correlation of NWHC with FLSA exceeds 0.8. Hence, the ability to predict the variations of NWHC, which are primarily associated with ENSO (Figs. 3a and 4), is tantamount to the ability to predict seasonal variations of the strength of the Leeuwin Current. We now explore predictive skill of NWHC anomalies using the Bureau of Meteorology coupled atmosphere-ocean seasonal forecast model POAMA (Predictive Ocean Atmosphere Model for Australia) and then develop a scheme to predict the Leeuwin Current by statistically downscaling the predictions of NWHC based on the historical relationship between FSLA and NWHC.

3.1 POAMA model

POAMA (Predictive Ocean Atmosphere Model for Australia) is the coupled atmosphere-ocean seasonal forecast model that is run operationally at the Bureau of Meteorology Australia (Alves et al. 2003). The atmospheric component of POAMA version 1.5 is based on the Bureau of Meteorology unified atmospheric model (BAM) version 3.0d. BAM is a spectral transform model, which is run here with triangular truncation 47 and 17 vertical levels. The ocean model is the Australia Community Ocean Model version 2 (ACOM2). It was developed from the Geophysical Fluid Dynamics Laboratory Modular Ocean Model version 2 (Pacanowski and Griffies 1998). The grid spacing is 2 degrees in the zonal direction. The meridional spacing is 0.5° within 8° of the equator, increasing gradually to 1.5° near the poles. There are 25 levels in the vertical, with 12 in the top 185 m. The maximum depth is 5,000 m. Technical details and some aspects of the performance of the ocean model, including the depiction of the Indonesian throughflow, are provided in Schiller et al. (1997) and Schiller et al. (2002). When run as part of a coupled climate model, the evolution of upper ocean heat content associated with ENSO, including the transmission through the

Indonesian throughflow and onto the west Australian coast, is faithfully captured (Zhong et al. 2005).

The ocean and atmosphere models are coupled using the Ocean Atmosphere Sea Ice Soil (OASIS) coupling software (Valcke et al. 2000) with no flux correction applied. Surface ocean currents are taken into account for computation of the surface stress that is provided to the ocean model. Coupling occurs every 3 hours.

Ocean initial conditions for the hindcasts are produced by an ocean data assimilation scheme (Wang et al. 2002) that is based on the optimum interpolation (OI) technique described by Smith et al. (1991a). Only temperature observations are assimilated and only measurements in the top 500 m are used. Corrections to currents are calculated by applying the geostrophic relation to the temperature corrections, similar to the method described by Burgers et al. (2002). Atmospheric initial conditions are provided by the Atmosphere-Land Initialization (ALI) scheme (Hudson and Alves 2007), which provides balanced atmosphere/land conditions for the BAM3 model based on ERA-40 reanalyzes (Uppala et al. 2005) for the period 1982-2002 and on operational analyses from the Bureau of Meteorology global weather forecast model for the period 2003-2006.

An ensemble of 10 members of hindcasts for start times January 1982 through December 2006 were then generated from the observed ocean and atmosphere initial conditions valid for the 1st of each month. The ensemble was generated by perturbing the atmospheric initial conditions by successively picking the atmospheric analysis from a 6 hour earlier period (i.e. the tenth member was initialized 2.5 days earlier than the first member). There was no perturbation applied to the ocean initial conditions. All forecasts were run for 9 months. We adopt the terminology that a lead time of 1 month means a forecast initialized on, for instance, 1 January that is valid for the month of

January. Forecast anomalies are formed relative to the forecast model climatology, which is a function of start month and lead time. In this fashion, the mean bias from the forecasts is removed.

3.2 Hindcast skill Nino34 and NWHC

The POAMA 1.5 system can predict the occurrence of ENSO up to 3 seasons in advance as demonstrated by the anomaly correlation and remote mean square error for the Nino34 SST index (Alves et al. 2003). The anomaly correlation remains above 0.7 and the normalized root mean square error remains below 1 at lead times out to 9 months. This ability to predict ENSO is reflected in the skill for predicting heat content anomalies throughout the equatorial central and east Pacific at lead times to 9 months (Fig. 5). High skill to lead time 9 months (correlation above 0.6) is also evident off the equator in the far west Pacific, which is associated with the slow westward propagating Rossby waves generated during ENSO. High skill is also seen on the northwest shelf of Australia. This high skill on the northwest shelf reflects the ability of POAMA to predict the oceanic teleconnection of ENSO from the Pacific, through the Indonesian throughflow and into the Indian Ocean. This is demonstrated in Fig. 3b, which shows the correlation of the time series of observed NWHC anomaly with the predicted heat content over tropical Pacific and Indian Oceans at 6 month lead time. The resemblance with the correlation between observed heat content anomaly and observed FSLA (Fig. 3a) is outstanding.

3.3 Downscaled predictions of the Leeuwin Current

In light of this ability to predict NWHC skilfully at lead time to 9 months and the tight coupling between NWHC and FLSA, we will now attempt to downscale the dynamical predictions of NWHC for prediction of the Leeuwin Current. Predictions of the seasonal variation of the Leeuwin Current, as expressed by variation of FSLA, are developed using predictions of the Nino34 SST index and NWHC directly from POAMA, together with the

historical relationship of FSLA with Nino34 SST and NWHC. We adopt a predictive scheme for FSLA at lead time τ from initial time t_0 of the form:

$$FSLA(t_0+\tau) = \alpha(t_0+\tau) \bullet FSLA(t_0) + \beta(t_0+\tau) \bullet Nino34^*(t_0+\tau) + \delta(t_0+\tau) \bullet HCNW^*(t_0+\tau) \quad (1)$$

Here we have allowed for the autocorrelation of *FSLA* (first term on right side) and for the strong associations of FSLA with Nino34 (second term) and with NWHC (third term). We include both Nino34 and NWHC as predictors because there maybe independent information contained in their predictions from POAMA. In (1) *Nino34**($t_0+\tau$) and *NWHC**($t_0+\tau$) are predictions directly from POAMA from initial time t_0 for a lead time τ. The regression coefficients β and δ *a*re obtained by least square fit of the simultaneous relationship of *observed FSLA* with *observed* Niño34 and NWHC indices, respectively, based on observed behavior 1982-2006. Computation of the regressions, which are a function of start month, and scoring of this predictive scheme were cross validated by successively leaving one year out, recomputing the regressions coefficients, and then generating the prediction.

Predictions of FSLA using (1) are shown in Fig. 2b for lead times 3, 6 and 9 months. All of the major fluctuations of FLSA are captured even out to lead time 9 months. The skill of this empirical downscaling scheme is quantified by the anomaly correlation (Figs. 6), which remains above 0.6 to 9 month lead time. While it is difficult to beat persistence of the initial FSLA at short lead times (1-3 months), this dynamical/empirical scheme readily beats persistence at longer lead times.

Subsequent analysis indicates that leaving out the dynamical prediction of either Nino34 or NWHC as predictors in (1), and then recomputing the regression coefficients, reduces the

skill by about 1 month lead time. Hence, while the bulk of the skill in predicting FSLA comes from using POAMA's predictions of either Nino34 or NWHC, they individually provide some independent information that can be exploited to make improved prediction of FSLA.

We have further compared (1) to a purely empirical scheme of the form

$$FSLA\,(t_0+\tau) = \alpha(t_0+\tau)\bullet FSLA\,(t_0) + \beta(t_0+\tau)\bullet Nino\,34(t_0) + \delta(t_0+\tau)\bullet HCNW\;(t_0) \qquad (2)$$

Here *Nino34*(t_0) and *NWHC*(t_0) are from observations at the initial time. The skill of this purely empirical scheme (2) is no better than persistence and thus is significantly less than that based on dynamical predictions of Nino34 and NWHC from POAMA using (1).

4. Conclusions

Skilful seasonal prediction of variations of the Leeuwin Current to nine month lead time was achieved by empirical downscaling of dynamical coupled model forecasts of the large-scale driver of the Leeuwin Current, namely the occurrence of ENSO and the associated variation of the south-north pressure gradient (upper ocean heat content gradient) in the eastern tropical-subtropical Indian Ocean. Prediction of the Leeuwin Current is possible because of the tight coupling of the interannual variations heat content on the north west shelf of Australia with ENSO. This coupling stems from the transmission of the upper ocean heat content anomaly in the western Pacific (high during La Niña and low during El Niño) through the Indonesian throughflow and southward onto the west Australian coast as a coastally trapped wave. The utility of these predictions have yet to be demonstrated, but the associated SST variations (and presumably salinity) along the west coast of Australia as a result of Leeuwin Current variations (Fig. 1b) suggest a wide range of application for management of fisheries and other aquatic resources.

The dynamical coupled model used here (POAMA) predicts with near-equal skill the occurrence of ENSO and the associated variation of heat content on the north west shelf of

Australia. Because of the tight coupling of the Leeuwin Current variations to ENSO in the Pacific, downscaled predictions of the current using dynamical predictions of ENSO in the equatorial Pacific (e.g., prediction of the Nino34 SST index) are as skilful as using dynamical predictions of heat content variations on the north west shelf of Australia. We demonstrated, however, that there is a modest amount of independent information in the dynamical predictions of Nino34 SST and the heat content on the north west shelf that can be exploited for improved prediction of the Leeuwin Current (i.e. forecast skill can be improved by about 1 month lead time if both are used).

The development of skilful prediction of the Leeuwin Current based on heat content variations on the north west shelf of Australia also emphasizes that there may be untapped predictability of the subsurface ocean that can be exploited for other applications. For instance, heat content in the south west equatorial Indian Ocean can be skilfully predicted to 9 month lead time (Fig. 5), which presumably stems from a teleconnection with ENSO associated with forced oceanic Rossby waves (Xie et al. 2002). The oceanic thermal response to these Rossby waves is associated with interannual variation of tropical cyclone activity (Xie et al. 2002). Thus, there may be untapped seasonal predictability of tropical cyclone activity based on skilful prediction of south equatorial Indian Ocean heat content that should be investigated.

Direct prediction of the Leeuwin Current with POAMA is not feasible because the resolution of the model is too coarse to fully resolve the current. But, we have shown that it is feasible to directly predict the large-scale driver of the variation of the Leeuwin Current, namely the south-north pressure gradient in the eastern Indian Ocean, using the dynamical coupled model forecasts. This is achieved because the coupled forecast model can skilfully predict ENSO in the Pacific and then can faithfully represent the transmission of the oceanic ENSO signal through the throughflow and onto the north west shelf of Australia. Although

our downscaled model for prediction of the Leeuwin Current, which uses dynamical predictions of both heat content on the north west shelf of Australia and Nino34 SST index, has only a modest increase in skill over that achieved from just predicting the occurrence of ENSO, direct skilful prediction of the variation of heat content on the north west shelf associated with ENSO is not necessarily a foregone conclusion. Depiction of the transmission of the oceanic El Niño signal through the Indonesian throughflow region and into the Indian Ocean is a challenge for climate models (e.g., Cai et al. 2005). The fact that we are able to predict heat content on the north west shelf with the current version of our dynamical forecast model suggests that direct prediction of the Leeuwin Current may be feasible in the future with improved model resolution and physics.

Acknowledgements

Monthly mean sea level at Fremantle was obtained from the Bureau of Meteorology National Tidal Centre. These data were derived from raw sea level measurements provided by the Fremantle Port Authority. Support for this work was provided in part from the the Western Australian Marine Science Institution (WAMSI) www.wamsi.org.au .

References

Alves, O., G. Wang, A. Zhong, N. Smith, F. Tseitkin, G. Warren, A. Schiller, S. Godfrey and G. Meyers, 2003: POAMA: Bureau of Meteorology operational coupled model seasonal forecast system. Proc. National Drought Forum, Brisbane, Apr 2003, pp. 49-56. Available from DPI Publications, Department of Primary Industries, GPO Box 46, Brisbane, Qld 4001, Australia.

Brankovic, C., and T. N. Palmer, and L. Ferranti, 1994: Predictability of seasonal atmospheric variations. *J. Climate,* **7,** 217–237.

Burgers, G., M. A. Balmaseda, F. C. Vossepoel, G. van Oldenborgh, P. van Leeuwen, 2002: Balanced Ocean-Data Assimilation near the Equator. *J. Phy. Oceanography*, **32**, 2509–2519.

Cai, W., H. H. Hendon, and G. Meyers, 2005: Indian Ocean dipolelike variability in the CSIRO Mark3 climate model. *J. Climate*, **18**, 1449-1468.

Clarke, A.J., and X. Liu, 1994: Interannual sea level in the northern and eastern Indian Ocean. *J. Phys., Oceanogr*., **24**, 1224-1235.

Feng, M., G. Meyers, A. Pearce, S. Wijffels, 2003: Annual and Interannual Variations of the Leeuwin Current at 32°S. *J. Geophys. Res.*, **108(11**), 3355, doi:10.1029/2002JC001763.

Hudson, D., and O. Alves, 2007: The impact of land-atmosphere initialisation on dynamical seasonal prediction. CAWCR Research Report No.133, Bur. Met., Melbourne, Australia, 4pp.

Goddard, L., S. J. Mason, S. E. Zebiak, C. F. Ropelewski, R. Basher, and M. A. Cane, 2001: Current approaches to seasonal-to-interannual climate predictions. *Int. J. Climatol*., **21**, 1111-1152.

Godfrey, J. S., and K. R. Ridgway, 1985: The large-scale environment of the poleward-flowing Leeuwin Current, Western Australia: Longshore steric height gradients, wind stresses, and geostrophic flow, *J. Phy. Ocean.*, **15**, 481-495.

Latif, M., D. Anderson, T. Barnett, M. Cane, R. Kleeman, A. Leetmaa, J. O'Brien, A. Rosati, and E. Scheider, 1998: A review of the predictability and prediction of ENSO. *J. Geophys. Res*., **103**, 14375-14393.

Legeckis, R., and G.R. Cresswell, 1981: Satellite observations of sea surface temperature fronts off the coast of western and southern Australia. *Deep-Sea Res*. **28A**, 297-306.

Pearce, A. F., and B. F. Phillips, 1988: ENSO events, the Leeuwin Current and larval recruitment of the western rock lobster, *J. Cons. Int. Explor. Mer.*, **45**, 13-21.

Pacanowski, R. C., and S. M. Griffies, 1998: *MOM 3.0 Manual*, NOAA/Geophysical Fluid Dynamics Laboratory, Princeton, USA 08542.

Reason, C.J.C., D. Gamble, and A.F. Pearce, 1999: the Leeuwin Current in the Parallel Ocean Climate Model and applications to regional meteorology and fisheries. *Meteorol. Appl*. **6**, 211-225.

Reynolds, R. W., N. A. Rayner, T. M. Smith, D. C. Stokes, and W. Wang, 2002: An Improved In Situ and Satellite SST Analysis for Climate. *J. Climate*, **15**, 1609-1625.

Schiller, A., J. S. Godfrey, P. McIntosh and G. Meyers, 1997: A global ocean general circulation model climate variability studies. CSIRO Marine Research Report No.227, 60 pp.

Schiller, A., J. S. Godfrey, P. C. McIntosh, G. Meyers, N. R. Smith, O. Alves, G. Wang and R. Fiedler, 2002: A New Version of the Australian Community Ocean Model for Seasonal Climate Prediction. CSIRO Marine Research Report No.240.

Shinoda, T., H.H. Hendon, M.A. Alexander, 2004a: Surface and subsurface dipole variability in the Indian Ocean and its relation to ENSO. *Deep Sea Res., I*, **51**, 619-635.

Shinoda, T., M.A. Alexander, H.H. Hendon, 2004b: Remote response of the Indian Ocean to interannual SST variations in the tropical Pacific. *J. Climate*, **17**, 362-372.

Smith, N. R., J. E. Blomley and G. Meyers, 1991a: A univariate statistical interpolation scheme for subsurface thermal analyses in the tropical oceans. *Prog. Oceanogr*., **28**, 219-256.

Smith, R.L. A. Huyer, J.S. Godfrey, and J. Church, 1991b: The Leeuwin Current off Western Australia, 1986-1987. *J. Phys., Oceanogr*., **21**, 323-345.

Stockdale, T. N., D. L. T. Anderson, J. O. S. Alves, and M. A. Balmaseda, 1998: Global seasonal rainfall forecasts using a coupled ocean-atmosphere model. *Nature*, **392**, 370-373.

Uppala, S. M., Kallberg, P. W., Simmons, A. J., Andrae, U., Da Costa Bechtold, V., Fiorino, M., Gibson, J. K., Haseler, J., Hernandez, A., Kelly, G. A., 2005: The ERA-40 re-analysis. *Quart. J. Roy. Meteor. Soc.*, **131(612)**, 2961-3012.

Valcke, S., L. Terray and A. Piacentini, 2000: OASIS 2.4 Ocean Atmospheric Sea Ice Soil users guide, Version 2.4. CERFACS Tech. Rep, CERFACS TR/CMGC/00-10, 85pp.

Wang, G., R. Kleeman, N. Smith, and F. Tseitkin, 2002: The BMRC coupled general circulation model ENSO forecast system. *Mon. Wea. Rev.*, **130**, 975-991.

Wiffels, S.and G. Meyers, 2003: An intersection of oceanic wave guides: Variability in the Indonesian throughflow region. *J. Phys. Oceanogr*., **34**, 1232-1253.

Xie, S.-P., H. Annamalai, F.A. Schott and J.P. McCreary, 2002: Structure and mechanisms of South Indian Ocean climate variability. *J. Climate*, 15, 864-878.

Zhong, A., H.H. Hendon, and O. Alves, 2005: Indian Ocean variability and its association with ENSO in a global coupled model. *J. Climate*, **18**, 3634-3649.

Figure Captions

Fig. 1 a) Long term mean SST (shading, interval 1°C) and vertical mean (upper 300 m) currents (vectors). The maximum poleward flowing current on the west coast has amplitude 3.2 cm s^{-1}. b) Regression of anomalous currents (vectors) onto the time series of Fremantle sea level anomaly (FSLA). Regressed current anomalies are scaled for a one standard deviations anomaly of FSLA. The maximum poleward flowing current anomaly on the west coast has magnitude 7.5 x 10^{-2} cm s^{-1}. Shading is correlation of SST with FSLA (shading level 0.1 with first level at 0.2).

Fig. 2 a) Monthly time series of Fremantle sea level anomaly (FSLA), Nino3.4 SST index (inverted), and observed NWHC (heat content averaged 15S-25S, 112E-120E). b) Observed and predicted FSLA at lead times 3, 6 and 9 months.

Fig. 3 Correlation of a) the monthly time series of FSLA with observed heat content from the POAMA assimilation and b) the monthly time series of observed NWHC with ensemble mean heat content at 6 month lead time for period 1982-2005. Shading interval for correlation is 0.15 with first level at ± 0.30. Zero correlation is indicated by heavy contour.

Fig. 4 Lag correlation of observed Nino3.4 SST index in DJF with heat content anomaly at a) lag 3 seasons (preceding MAM), b) lag 2 seasons (preceding JJA), c) lag 1 season (preceding SON) and d) simultaneous. Correlation is plotted as in Fig. 3.

Fig. 5 Anomaly correlation of predicted heat content at lead time a) 3 months, b) 6 months, and c) 9 months for POAMA hindcasts 1982-2005. Correlation is plotted as in Fig. 3.

Fig. 6 Anomaly correlation as a function of forecast lead time for FSLA (heavy black curve) using (1). Also shown is the skill for persistence (dashed curve) and for predictions using just Nino3.4 (red) or NWHC (green). Correlation is computed using ensemble mean of forecasts of Nino34 and NWHC from POAMA for the period 1982-2005.

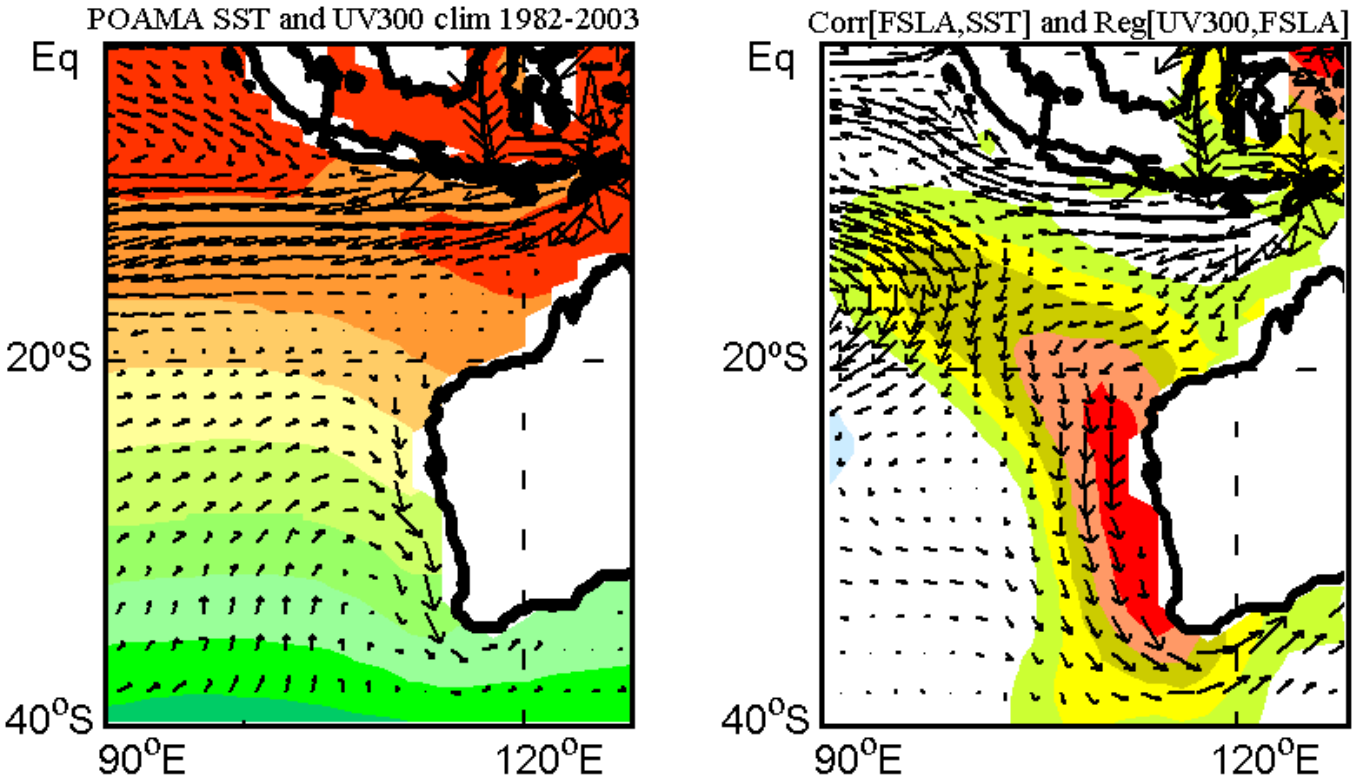

Fig. 1 a) Long term mean SST (shading, interval 1°C) and vertical mean (upper 300 m) currents (vectors). The maximum poleward flowing current on the west coast has amplitude 3.2 cm s^{-1}. b) Regression of anomalous currents (vectors) onto the time series of Fremantle sea level anomaly (FSLA). Regressed current anomalies are scaled for a one standard deviations anomaly of FSLA. The maximum poleward flowing current anomaly on the west coast has magnitude 7.5 x 10^{-2} cm s^{-1}. Shading is correlation of SST with FSLA (shading level 0.1 with first level at 0.2).

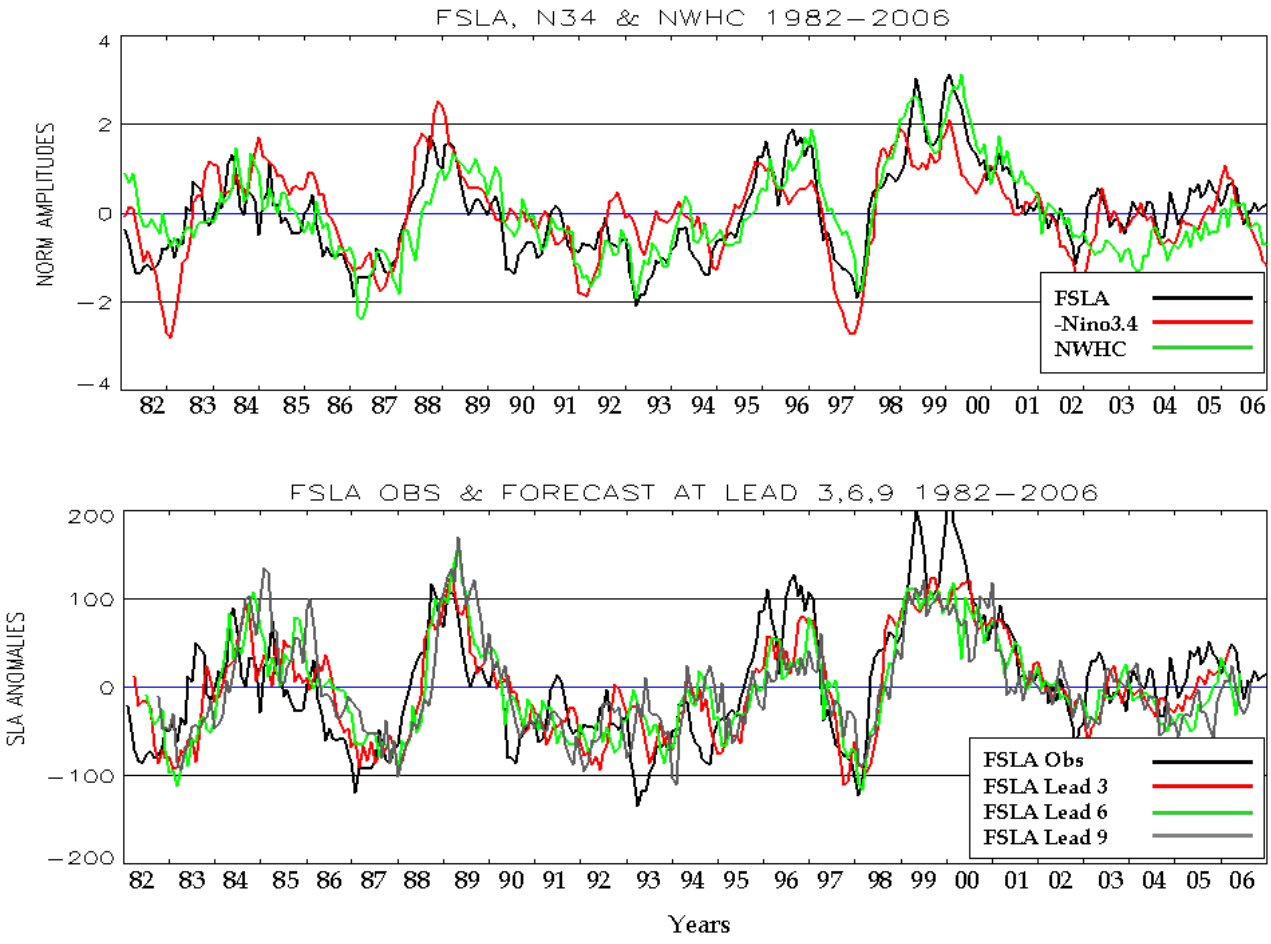

Fig. 2 a) Monthly time series of Fremantle sea level anomaly (FSLA), Nino3.4 SST index (inverted), and observed NWHC (heat content averaged 15S-25S, 112E-120E). b) Observed and predicted FSLA at lead times 3, 6 and 9 months.

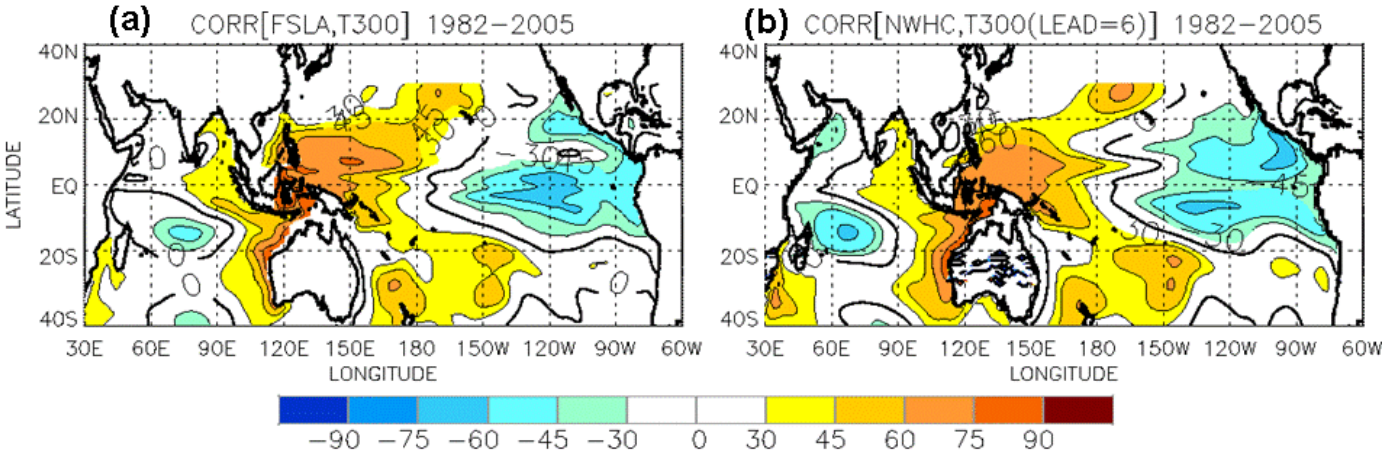

Fig. 3 Correlation of a) the monthly time series of FSLA with observed heat content from the POAMA assimilation and b) the monthly time series of observed NWHC with ensemble mean heat content at 6 month lead time for period 1982-2005. Shading interval for correlation is 0.15 with first level at ± 0.30. Zero correlation is indicated by heavy contour.

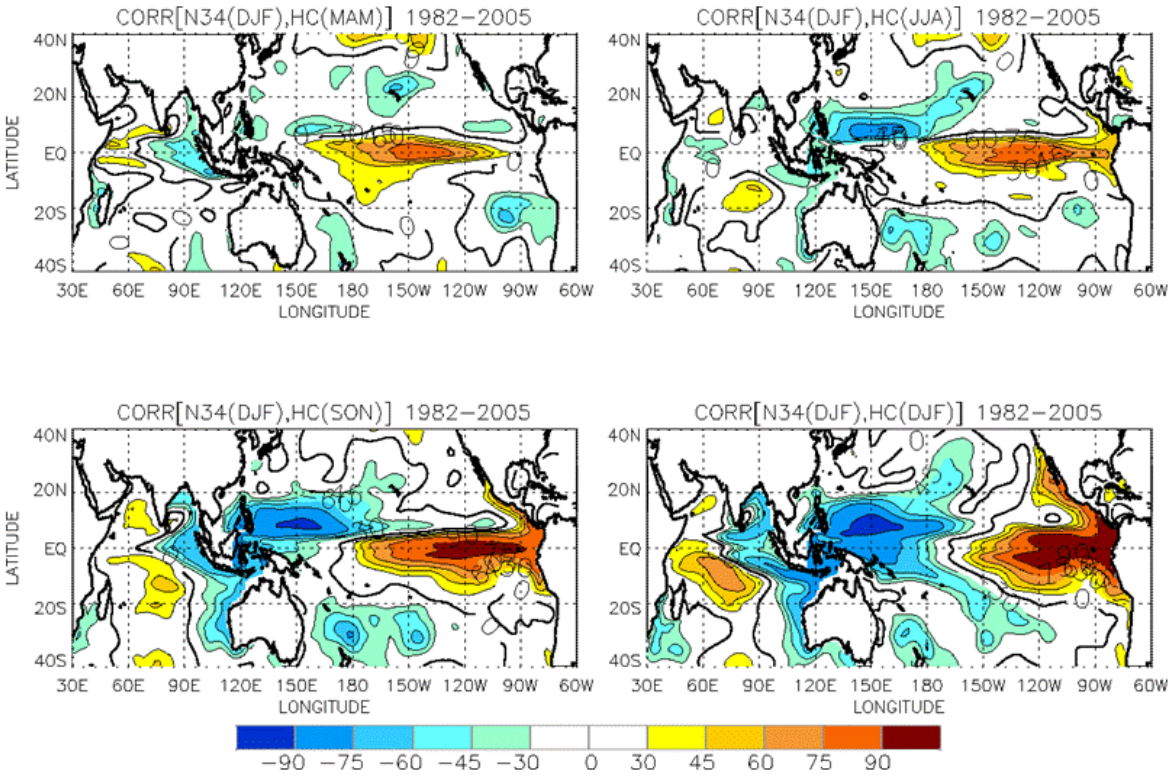

Fig. 4 Lag correlation of observed Nino3.4 SST index in DJF with heat content anomaly at a) lag 3 seasons (preceding MAM), b) lag 2 seasons (preceding JJA), c) lag 1 season (preceding SON) and d) simultaneous. Correlation is plotted as in Fig. 3.

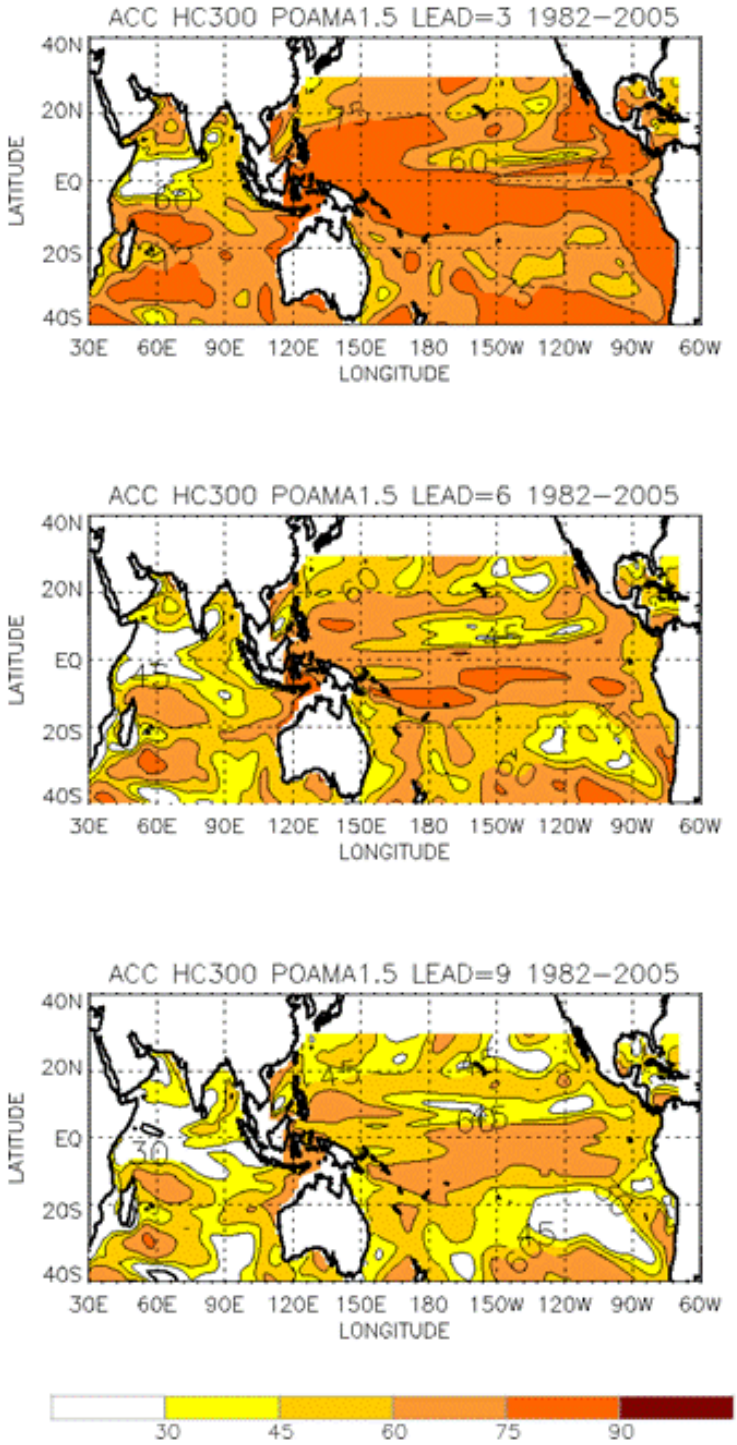

Fig. 5 Anomaly correlation of predicted heat content at lead time a) 3 months, b) 6 months, and c) 9 months for POAMA hindcasts 1982-2005. Correlation is plotted as in Fig. 3.

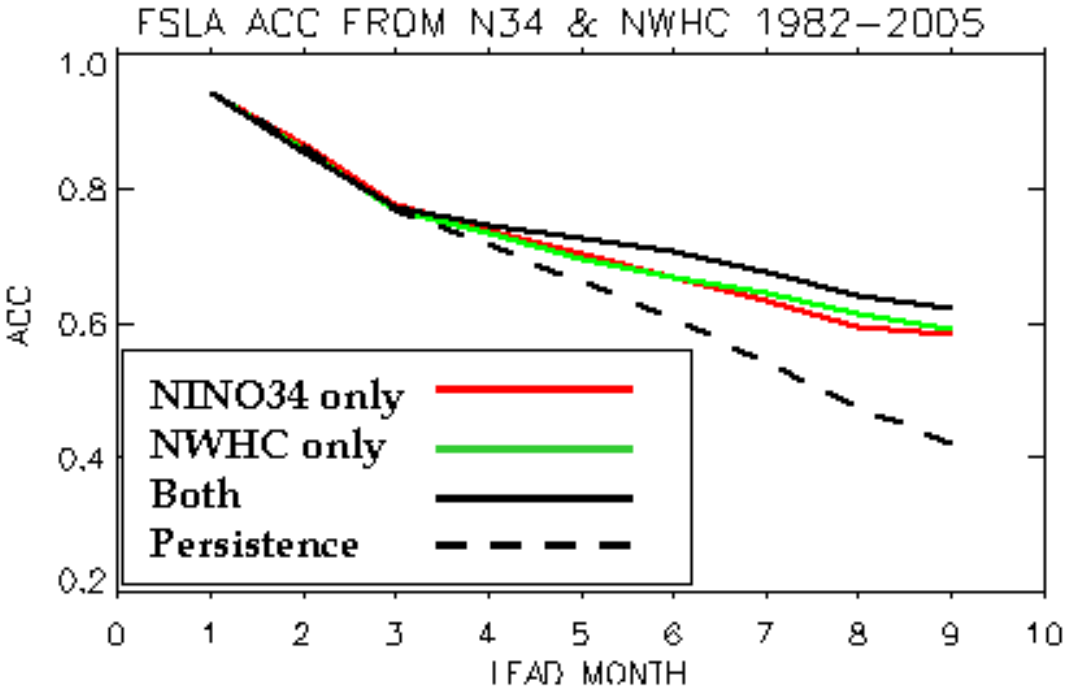

Fig. 6 Anomaly correlation as a function of forecast lead time for FSLA (heavy black curve) using (1). Also shown is the skill for persistence (dashed curve) and for predictions using just Nino3.4 (red) or NWHC (green). Correlation is computed using ensemble mean of forecasts of Nino34 and NWHC from POAMA for the period 1982-2005.